

Estimating Orbital Parameters of Direct Imaging Exoplanet Using Neural Network

Bo Liang^{1,2*}, Hanlin Song^{3,*}, Chang Liu¹, Tianyu Zhao¹, Yuxiang Xu^{1,4,2}, Zihao Xiao^{1,5}, Manjia Liang¹, Minghui Du¹, Wei-Liang Qian⁶, Li-e Qiang^{1,5}, Peng Xu^{1,7,2,8}, Ziren Luo^{1,7,2}

*These authors contributed equally to this work.

¹Center for Gravitational Wave Experiment, National Microgravity Laboratory, Institute of Mechanics, Chinese Academy of Sciences, Beijing, 100190, China.

²Taiji Laboratory for Gravitational Wave Universe (Beijing/Hangzhou), University of Chinese Academy of Sciences (UCAS), Beijing, 100049, China.

³School of Physics, Peking University, Beijing, 100871, China.

⁴Shanghai Institute of Optics and Fine Mechanics, Chinese Academy of Sciences, Shanghai, 201800, China.

⁵National Space Science Center, Chinese Academy of Sciences, Beijing, 100190, China.

⁶Escola de Engenharia de Lorena, Universidade de São Paulo, Lorena, 12602-810, SP, Brazil.

⁷Key Laboratory of Gravitational Wave Precision Measurement of Zhejiang Province, Hangzhou Institute for Advanced Study, UCAS, Hangzhou, 310024, China.

⁷Lanzhou Center of Theoretical Physics, Lanzhou University, Lanzhou, 730000, China.

Contributing authors: zhaotianyu@imech.ac.cn; xupeng@imech.ac.cn;

Abstract

In this work, we propose a new flow-matching Markov chain Monte Carlo (FM-MCMC) algorithm for estimating the orbital parameters of exoplanetary systems, especially for those only one exoplanet is involved. Compared to traditional methods that rely on random sampling within the Bayesian framework, our approach first leverages flow matching posterior estimation (FMPE) to efficiently constrain the prior range of physical parameters, and then employs MCMC to accurately infer the posterior distribution. For example, in the orbital parameter inference of β Pictoris b, our model achieved a substantial speed-up while maintaining comparable accuracy—running 77.8 times faster than Parallel Tempered MCMC (PTMCMC) and 365.4 times faster than nested sampling. Moreover, our FM-MCMC method also attained the highest average log-likelihood among all approaches, demonstrating its superior sampling efficiency and accuracy. This highlights the scalability and efficiency of our approach, making it well-suited for processing the massive datasets expected from future exoplanet surveys. Beyond astrophysics, our methodology establishes a versatile paradigm for synergizing deep generative models with traditional sampling, which can be adopted to tackle complex inference problems in other fields, such as cosmology, biomedical imaging, and particle physics.

1 Introduction

Since the first confirmed detection of an exoplanetary system in 1992 [1] and the first confirmed detection of an exoplanet in 1995 [2], more than 4,615 exoplanetary systems and 5,989 exoplanets have been confirmed as of September 2025 [3]. These systems exhibit a wide range of characteristics, including variations in the number and composition of exoplanets, the dynamics of their orbital motions, and the types of their host stars. Notably, the majority of these systems are characterized by the detection of only a single planet, although this is partly due to observational biases. For a recent review, see, e.g., Ref. [4]. Thus, high-precision exoplanet detectors are essential for investigating the mechanisms underlying these characteristics, such as testing theories of planet formation and migration, and understanding the overall evolution of planetary systems [5, 6]. Currently, several observatories remain in operation and are continuously expanding our exoplanet census. Operational projects like Transiting Exoplanet Survey Satellite (TESS) [7] and Characterising ExO-Planets Satellite (CHEOPS) [8] conduct high-precision photometric surveys of nearby bright stars, enabling the detection

and characterization of transiting exoplanets. In parallel, Gaia [9] ultra-precise astrometric data that reveals subtle stellar motions caused by orbiting planets. Additionally, instruments like Spectro-Polarimetric High-contrast Exoplanet REsearch instrument (SPHERE) [10] on the Very Large Telescope (VLT) directly image exoplanets, offering valuable constraints on their orbital architectures and atmospheric properties. Upcoming missions such as PLAnetary Transits and Oscillations of stars (PLATO) [11], Atmospheric Remote-sensing Infrared Exoplanet Large-survey (ARIEL) [12, 13], SPHERE+ [14], and Nancy Grace Roman Space Telescope [15] are expected to significantly advance our understanding of exoplanet populations. By integrating large-scale photometric monitoring, atmospheric spectroscopy, and precise astrometric measurements, these missions are poised to deliver unprecedented insights into the formation, evolution, and diversity of planetary systems.

In recent years, a variety of exoplanet discovery techniques have been developed and extensively employed [16], including transit photometry, radial velocity (RV), microlensing, and direct imaging. These efforts have led to the detection of a large number of exoplanetary systems, significantly advancing our understanding of the statistical properties of planetary populations and providing critical constraints on models of planet formation and migration. In this work, we focus on exoplanetary systems detected using direct imaging method. Although the number of such detections is smaller than that obtained with the other three techniques [17, 18], direct imaging provides unique advantages for determining the demographics of exoplanets around nearby young stars, characterizing their atmospheric properties, and exploring their circumstellar disks [14]. Through synergy with other facilities, such as Gaia, GRAVITY [19], and James Webb Space Telescope (JWST) [20], more exoplanets will be directly imaged. This growing catalog of directly imaged exoplanets will yield essential observational data, which is vital for testing and validating theoretical models of planet formation and evolution, thereby elucidating the fundamental physical processes that determine planetary system architectures.

With the growing accumulation of observational data, a key challenge lies in the rapid and precise estimation of the physical parameters of exoplanetary systems, which are crucial for predicting exoplanet locations, calculating transit probabilities, and assessing the climates and habitability of Earth-like worlds in future missions. In the case of directly imaged exoplanets, several approaches have been proposed for estimating the physical parameters [5], such as linearized least square adjustment [21], the Orbits for the Impatient (OFTI) algorithm [22] and the Parallel Tempered Markov Chain Monte Carlo (PTMCMC) algorithm [23, 24]. Tools such as `orbitize!` implement Nested Sampling [25], and have been demonstrated in studies that combine astrometric and radial velocity data to constrain exoplanet orbits [5, 6]. However, these traditional methods [21–24] suffer from limitations: Due to high parameter dimensionality and the potential multimodality of posterior distributions, convergence can be prohibitively slow without an optimal proposal distribution or favorable random initialization. In contrast, while machine learning based methods [26–28] offer a significant advantage in speed for rapid orbital parameter inference, the posterior distributions they generate typically exhibit larger errors than traditional MCMC methods and often fail to accurately capture multimodality. Consequently, achieving rapid inference of exoplanet orbital parameters while maintaining high precision remains a pressing challenge.

Recent advances in deep learning have enhanced exoplanet studies by improving the detection and analysis of observational data across various missions [29–33]. Convolutional neural networks effectively identify subtle transit signals in light curves from missions such as Kepler [34–36] and TESS [37, 38], while deep learning approaches applied to radial velocity and direct imaging data help reduce noise and reveal faint planetary features. Generative models like normalizing flows [39–42] and neural ordinary differential equations [43–46] provide efficient tools for simulation-based inference (SBI) [47, 48], reducing computational requirements compared to traditional methods. Additionally, recurrent neural networks and long short-term memory models capture temporal patterns in the data [49, 50], improving the analysis of transit timing variations and other dynamic effects. By integrating photometric, spectroscopic, and spectrometric observations, these deep learning techniques could offer more robust and comprehensive exoplanet characterization [51, 52].

In this work, we present a novel approach, *flow-matching enhanced MCMC* (FM-MCMC), which leverages continuous normalizing flows (CNFs) [44] trained via a flow-matching objective [47, 53, 54] to accelerate MCMC sampling. Our method achieves posterior estimates that closely approximate those obtained by PTMCMC and nested sampling, while outperforming neural posterior estimation [55, 56] in precision. FM-MCMC combines the robustness and interpretability of traditional MCMC sampling with the computational speed of normalizing flow, yielding higher posterior accuracy than standalone SBI methods [57–59]. The key innovation of FM-MCMC lies in its hybrid architecture: it first uses a CNFs, trained efficiently via flow matching, to rapidly learn a high-quality proposal distribution that closely approximates the true posterior. This flow-generated proposal is then injected into a PTMCMC sampler, substantially improving convergence by providing optimal starting points and reducing the burn-in phase to just 1% of the traditional requirement. It is worth emphasizing that FM-MCMC is a widely applicable algorithm for accelerating parameter inference in scientific problems. In this work, we focus on its application to directly imaged exoplanetary systems, enabling rapid extraction of orbital parameters from observational data. As a results, a flow-matching based neural network is trained with 16 million simulated exoplanetary systems observational data. We then apply this model to infer the orbital parameters of β Pictoris b, the first exoplanet discovered via direct imaging [60, 61]. Compared to traditional parameter estimation methods, FM-MCMC provides up to a 77.8 \times speedup over nested sampling, and a 365.4 \times speedup over nested sampling. This algorithm demonstrates a substantial speedup while maintaining the accuracy of parameter estimates, highlighting the significant potential of FM-MCMC for orbital parameter inference of direct imaged exoplanetary system.

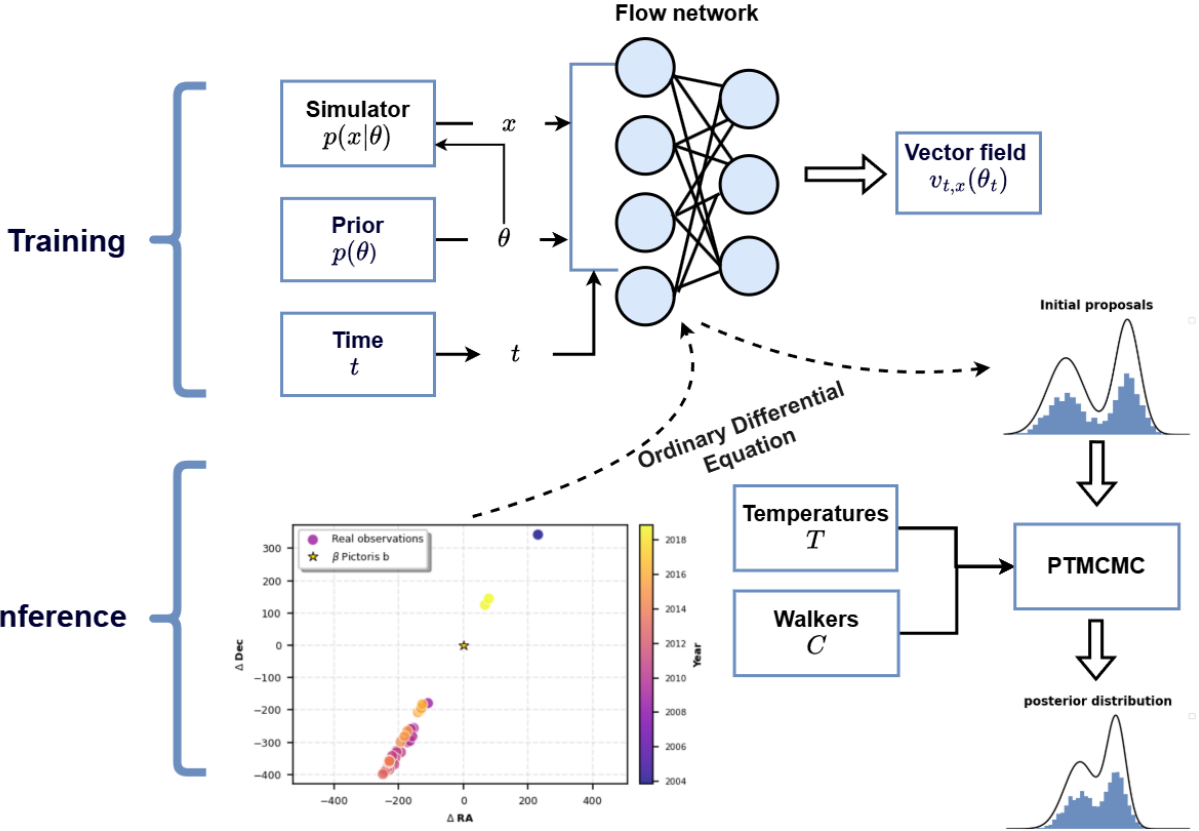


Fig. 1 Flow-matching MCMC framework. In the Training section, there is first a prior distribution $p(\theta)$, from which the parameter θ is extracted, and the data is generated by a model x . These generated data are fed into the training process along with the parameters. The inference section is based on the trained model, input the real observation data, and use the trained model to infer the initial proposals. The initial proposal is then provided to PTMCMC for likelihood calculations.

The remainder of this paper is organized as follows. In Section 2, we present the FM-MCMC methodology. Section 3 describes the experimental setup and the simulated astrometric data used for training. In Section 4, we present our results and discuss the implications for exoplanet orbit characterization. Finally, Section 5 summarizes our conclusions and outlines prospects for future work.

Table 1 The prior distributions of eight orbital parameters.

Parameter	Description	Priors
a	The semi-major axis is half of the orbit's longest diameter.	Log-uniform(4, 40) au
e	The eccentricity describes the shape of the orbit.	Uniform(10^{-5} , 0.99)
i	The inclination angle determines the position of the planet in orbit.	Sine(81° , 99°)
ω	Argument of periastron describes the orientation of the orbital plane.	Uniform(0° , 360°)
Ω	Longitude of ascending node describes the orientation of the orbital plane.	Uniform(25° , 85°)
τ	Epoch of periastron passage describes the position of a planet in orbit.	Uniform(0, 1)
π	Parallax measures the distance between a star and the Earth.	$\mathcal{N}(51.44, 0.12)$ mas
M_T	Total mass describes the total mass of the stars and planets.	$\mathcal{N}(1.75, 0.05)$ M_\odot

2 Flow-matching enhanced Markov chain Monte Carlo

In this section, we introduce the FM-MCMC algorithm to accelerate posterior sampling. Based on the CNFs and flow matching algorithm, we first train a neural network for initial inference. Then, along with the PTMCMC, we obtain the accurate posterior distributions. Unlike traditional MCMC methods—which often suffer from slow convergence in high-dimensional and multi-modal parameter spaces due to inefficient proposal mechanisms and sensitivity to initial conditions—FM-MCMC leverages a learned flow-based proposal that drastically reduces the number of likelihood evaluations and shortens burn-in phases. The proposed FM-MCMC framework builds on two key developments in machine learning-based inference: SBI and flow matching. In particular, flow matching [53, 54] offers a highly efficient objective

for training CNFs, which was recently adapted for SBI by Dax et al. [47] to enable fast posterior estimation. FM-MCMC approach retains the statistical robustness and interpretability of traditional Bayesian sampling while harnessing the expressivity and computational efficiency of normalizing flows. Importantly, the FM-MCMC paradigm is not limited to astrophysical applications; its general structure allows for adoption across a wide range of scientific inference problems, including those in cosmology, particle physics, and biomedical modeling, where rapid and accurate posterior estimation is essential.

2.1 Continuous normalizing flows

Generative models are designed to learn invertible transformations that map high-dimensional data distributions to simpler reference distributions. Notably, Normalizing Flows achieve exact density estimation by applying the chain rule to compositions of invertible functions. However, their discrete layer-wise architecture limits their capacity to model highly complex data distributions. To overcome this limitation, CNFs were introduced. CNFs construct a time-dependent probability density path $p_t(\theta)$ governed by a neural network-parameterized vector field $v_t(x; \theta)$. The evolution of samples in CNFs is described by an ordinary differential equation (ODE):

$$\frac{d}{dt} \phi_{t,x}(\theta) = v_{t,x}(\phi_{t,x}(\theta)), \quad v_{t=0,x}(\theta) = \theta_0, \quad v_{t=1,x}(\theta) = \theta_1. \quad (1)$$

Traditional methods optimize the model via maximum likelihood estimation by minimizing the negative log-likelihood. However, backpropagation through an ODE solver incurs a computational cost of $O(d^3)$, where d denotes dimensionality, hindering scalability to high-dimensional data.

Flow Matching (FM) offers a solution by introducing a more efficient optimization objective. In contrast to conventional CNFs, FM decouples the probability density path from the underlying dynamics, substantially reducing computational overhead. It explicitly constructs a target probability path $p_t(\theta)$ and its associated velocity field $u_t(\theta)$, and trains a parametric velocity field $v_{t,x}(\theta)$ to approximate $u_t(\theta)$. Dax et al. applied FM to simulation-based inference, proposing a highly efficient training objective that alleviates the computational demands of traditional methods.

The method begins by defining a Gaussian probability path conditioned on a target parameter θ_1 :

$$p_t(\theta | \theta_1) = \mathcal{N}(\theta | \theta_1 t, (1-t)^2 I_d), \quad (2)$$

which ensures the distribution starts as a standard normal $\mathcal{N}(0, I_d)$ at $t = 0$ and converges to a Gaussian centered at θ_1 when $t = 1$. The corresponding conditional velocity field that generates this path is derived as:

$$u_t(\theta | \theta_1) = \theta_1 - \theta, \quad (3)$$

enabling linear transport of samples from the base to the target distribution over time.

To approximate the posterior, the framework marginalizes over target parameters $\theta_1 \sim p(\theta)$ and conditions on observed data $x \sim p(x | \theta_1)$, yielding an aggregate probability path $p_t(\theta)$ and a composite velocity field $u_t(\theta)$ such that $p_1(\theta) = q(\theta | x)$. The training objective minimizes the mean-squared error between the learned and true velocity fields:

$$\mathcal{L}_{\text{FMPE}} = \mathbb{E}_{t \sim \mathcal{U}(0,1)} \mathbb{E}_{\theta_1 \sim p(\theta)} \mathbb{E}_{x \sim p(x | \theta_1)} \mathbb{E}_{\theta_t \sim p_t(\theta_t | \theta_1)} \|v_{t,x}(\theta_t) - u_t(\theta_t | \theta_1)\|^2. \quad (4)$$

This regression-based approach avoids expensive backpropagation through ODE solvers, greatly improving scalability in high-dimensional settings. Once trained, posterior samples are generated by solving the ODE numerically, effectively transforming base distribution samples into draws from the approximate posterior.

2.2 Flow-matching Markov chain Monte Carlo

The FM-MCMC algorithm first employs CNFs trained through flow matching to enable rapid obtaining the initial proposals to efficiently generate initial proposals tailored to specific scientific problems. These proposals are then refined using PTMCMC to obtain accurate posterior distributions.

For example, when applying the FM-MCMC algorithm to estimate the orbital parameters of imaged exoplanet, i.e. β Pictoris b, a two-step inference is performed,

- Step 1. Obtain the initial proposal for the orbital parameters of β Pictoris b using a pretrained neural network. This network is trained on $O(10^6)$ simulated exoplanetary orbital observations with predefined true parameters.
- Step 2. Obtain the accurate posterior distribution with the injected initial proposal using the PTMCMC algorithm.

The CNFs sample production dynamically adapts to PTMCMC's chain configurations and temperature ladder parameters. This integration delivers two key enhancements: (1) Using CNFs posterior samples as the initialization proposal distribution, and (2) Burn-in phases are reduced to 1% of the original requirement. Final posterior distributions are derived from thermally equilibrated PTMCMC chains. Consequently, efficient and accurate posterior sampling is achieved. Our FM-MCMC method **Key innovation** are *Flow-based proposal distribution*: normalizing flows generate high-quality candidate samples, minimizing redundant state exploration; *Hybrid hardware parallelism*: GPU accelerates flow model training while CPU handles parallel annealing, optimizing resource utilization. Implemented on Pytorch with

GPU-CPU co-processing, FM-MCMC reduces hour-scale tasks (e.g., generating 10,000 samples) to minutes, enabling real-time high-dimensional inference.

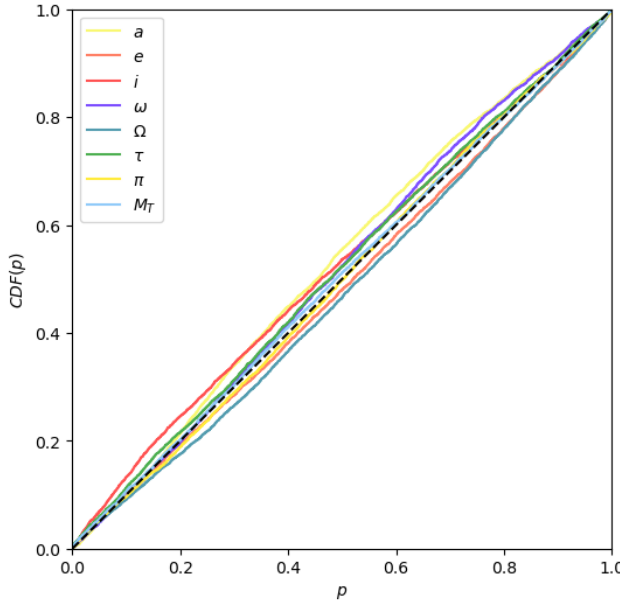


Fig. 2 P-P plot validating the unbiasedness of the CNF model. The near-perfect alignment of all CDF curves (colored lines) with the theoretical diagonal $y=x$ (black dashed line) indicates statistical consistency between the CNF posterior estimates and the true distribution.

3 Flow-matching enhanced neural network

With the FM-MCMC algorithm and a training dataset tailored to a specific scientific problem, a powerful flow-matching based neural network for posterior estimation can be obtained. At present, we focus on inferring the orbital parameters of directly imaged exoplanetary systems, specifically in cases where only a single exoplanet is involved. In this section, we first describe the datasets employed for model training and evaluation, grounded in observational data from directly imaged exoplanets. We then present the model architecture and training procedures in detail.

3.1 Dataset generation

Since our ultimate goal is to estimate the orbital parameters of β Pictoris b with the trained neural network, it is essential to construct a training dataset consisting of simulated observations that closely resemble systems analogous to β Pictoris b. In this work, we generate a dataset comprising 16 million simulated orbital configurations.

The β Pictoris b was the first exoplanet discovered through direct imaging, using the NaCo adaptive optics instrument on the European Southern Observatory's VLT [60, 61]. With follow-up observations from The Gemini NICI Planet-Finding Campaign [62], SPHERE at the VLT [63], and Gemini Planet Imager (GPI) [64], the detailed properties of β Pictoris b have been characterized. It is confirmed as a giant gas planet with a mass of approximately $12.8 M_{\text{Jup}}$, on an eccentric orbit at a semi-major axis of 10.2 astronomical units (au), around the 10-million-year-old β Pictoris system [64]. Even when accounting for the observational data of the recently discovered inner giant planet, β Pictoris c [65], detected via radial velocity measurements and orbiting at 2.7 au, no significant differences are observed in the inferred orbital parameters of β Pictoris b [64]. Therefore, in this work, we focus solely on the primary planet, β Pictoris b, in its system.

The relative astrometry data of exoplanets are often expressed as the star-planet separation and position angle, or equivalently as the relative right ascension (ΔRA) and relative declination (ΔDec) [6, 64]. These observed orbital data can be parameterized with eight quantities [66]: the six standard Keplerian elements—including semi-major axis a , eccentricity e , inclination i , argument of periastron ω , longitude of ascending node Ω , time of periastron τ —as well as the parallax π , and total system mass M_{tot} . The training dataset is generated as follow:

- We first generate 16 million orbital configurations by sampling from the prior ranges specified in Table 1. Notably, a sine prior is adopted for the inclination to ensure an isotropic and uniform distribution over the celestial sphere [6].
- For each configuration, the relative astrometry data ΔRA and ΔDec is obtained with the relevant eight parameters through Kepler's law. We utilize the `calc_orbit`¹ function in the open-source software package `orbitize!` [6] for calculation.

¹<https://github.com/sblunt/orbitize/tree/main>

- Finally, Gaussian noise $\mathcal{N}(0, \epsilon)$ is added to synthetic data for realism: $\Delta\text{RA}_{\text{noisy}} = \Delta\text{RA} + \mathcal{N}(0, \epsilon_{\text{RA}})$ and $\Delta\text{Dec}_{\text{noisy}} = \Delta\text{DEC} + \mathcal{N}(0, \epsilon_{\text{Dec}})$, where ϵ_{RA} and ϵ_{Dec} are calibrated from observations of β -Pictoris b [64].

The final dataset comprises 16 million samples, each containing:

- Time-series data $\Delta\text{RA}_t, \Delta\text{Dec}_t$, which are each vectors of length 34, resulting in a combined input dimension of 68.
- Ground-truth labels: $\{a, e, i, \omega, \Omega, \tau, \pi, M_{\text{T}}\}$

This facilitates supervised learning of the inverse problem, namely mapping astrometric signals to orbital parameters.

3.2 Model building and training

The architecture of neural network is composed of an embedding network and a flow network. The embedding network projects the inputs into a 68-dimensional latent space, preserving essential information while improving computational efficiency. Meanwhile, the flow network—constructed with 21 residual blocks arranged in a pyramidal structure—progressively compresses features from 68 to 8 dimensions. This hierarchical design enables the effective fusion of the embedded tuple (x, t, θ_t) and ultimately facilitates high-precision prediction of the vector field $v_{t,x}(\theta_t)$.

The training employed early stopping to mitigate overfitting, with an initial learning rate of 0.0001 adjusted by a cosine annealing schedule. Using an NVIDIA RTX 4090 GPU, each epoch required approximately 30 seconds, and optimal convergence was achieved after 46 epochs. Owing to the efficiency of flow-matching techniques, the entire training process was completed in just 22 minutes. To statistically validate the calibration of the CNFs architecture across the full parameter space, Figure 2 presents a Probability-Probability (P-P) plot demonstrating the model’s unbiasedness, where all parameter-wise cumulative distribution functions (CDFs) align closely with the theoretical diagonal. This consistency highlights the unbiased nature of the trained model, confirming its reliability and robustness across diverse parameters.

4 Results

With the flow-matching-based neural network, the orbital parameters of β Pictoris b can be inferred through the two-step procedure described above. First, the neural network provides an initial proposal for the eight orbital parameters. Next, the accurate posterior distribution is obtained by injecting this initial proposal into the PTMCMC algorithm. Our FM-MCMC results demonstrate two major improvements over previous parameter estimation methods that rely solely on either machine learning or traditional sampling algorithms. Specifically, FM-MCMC not only achieves higher accuracy in estimating the orbital parameters compared to methods that rely solely on NPE—reducing biases and better capturing the true posterior distributions, but also demonstrates substantially improved computational efficiency relative to traditional sampling algorithms, such as nested sampling or PTMCMC, by requiring fewer likelihood evaluations and converging faster to the target posterior. This combination of enhanced precision and efficiency makes FM-MCMC a particularly powerful approach for accurate and practical parameter estimation in exoplanetary orbital studies.

4.1 Accuracy improvement compared with neural posterior estimation

Current applications of machine learning to exoplanetary orbital parameter estimation can be broadly classified into two primary approaches. One line of work employs Deep Probabilistic Inference (DPI), where the use of restricted prior ranges enhances computational efficiency but comes at the cost of reduced posterior exploration [26]. Another line adopts NPE, which enables rapid generation of posterior distributions through amortized inference. However, comparative analyses indicate that NPE-derived posteriors generally exhibit broader uncertainty bounds than those obtained with traditional MCMC sampling in exoplanetary orbit recoveries [27]. Recent research has shown that, given the same prior range for inferring β Pictoris b orbital parameters, NPE attains a more accurate posterior distribution than DPI [27]. Building on this improvement, we further demonstrate that, under identical conditions, the posterior accuracy achieved by NPE, while superior to DPI, still does not reach the level attained by FM-MCMC.

For a fair comparison, the NPE model is trained on the same dataset of 16 million samples while adopting identical hyperparameter settings as FM-MCMC. When applied to the observational data of β Pictoris b, the resulting posterior distributions obtained with NPE and FM-MCMC are presented in Figure 3. As can be seen, across all eight orbital parameters the constraints provided by NPE are systematically weaker, and for parameters such as the semi-major axis, eccentricity, and argument of periastron, an undesirable degeneracy arises. This demonstrates that the proposed FM-MCMC method not only achieves higher accuracy but also provides greater interpretability, thereby representing a more advanced and reliable alternative to existing deep learning approaches.

4.2 Efficiency improvement compared with PTMCMC and Nested sampling

To rigorously evaluate the effectiveness of FM-MCMC, we performed posterior estimation for β Pictoris b using both PTMCMC and Nested sampling. The PTMCMC sampler was configured with 20 temperature tiers and 1,000 parallel

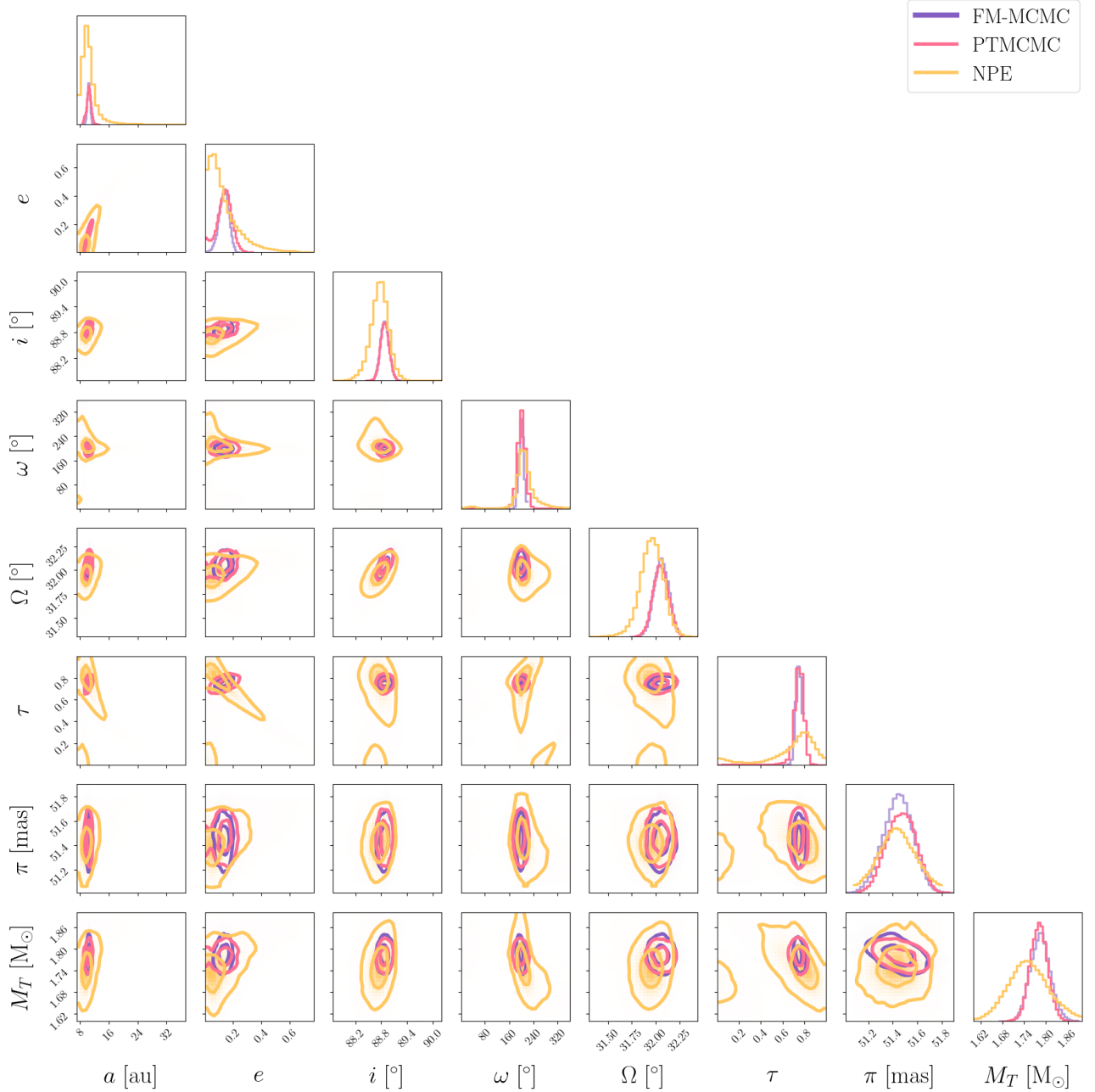


Fig. 3 FM-MCMC vs PTMCMC vs NPE posterior comparison for β Pictoris b orbital elements. Comparative analyses reveal that NPE produces broader posterior distributions, whereas FM-MCMC delivers more concentrated estimates, underscoring its superior statistical precision.

chains. After burn-in, we retained the final 10,000 samples for posterior analysis. Both samplers utilized parallel computing with 10 threads, implemented on an AMD Ryzen 9 7945HX CPU. The PTMCMC computation completed in 452 minutes, while the Nested sampling algorithm required 2124 minutes to achieve convergence.

Table 2 Comparison of efficiency and effectiveness of different posterior sampling approaches.

Sampling Method	Runtime (seconds) \uparrow	Speedup Ratio ($t/t_{\text{FM-MCMC}}$)	Likelihoods (mean [max]) \uparrow
FM-MCMC (ours)	348.9	1	-133.0 [-129.6]
PTMCMC	27133.9	77.8	-285.4 [-129.6]
Nested sampling	127478.8	365.4	-234.3 [-129.5]

FM-MCMC demonstrates statistical robustness in parameter inference. As shown in Fig.4, both the 2D contours and 1D marginal distributions of all FM-MCMC parameters, along with the corresponding confidence intervals listed

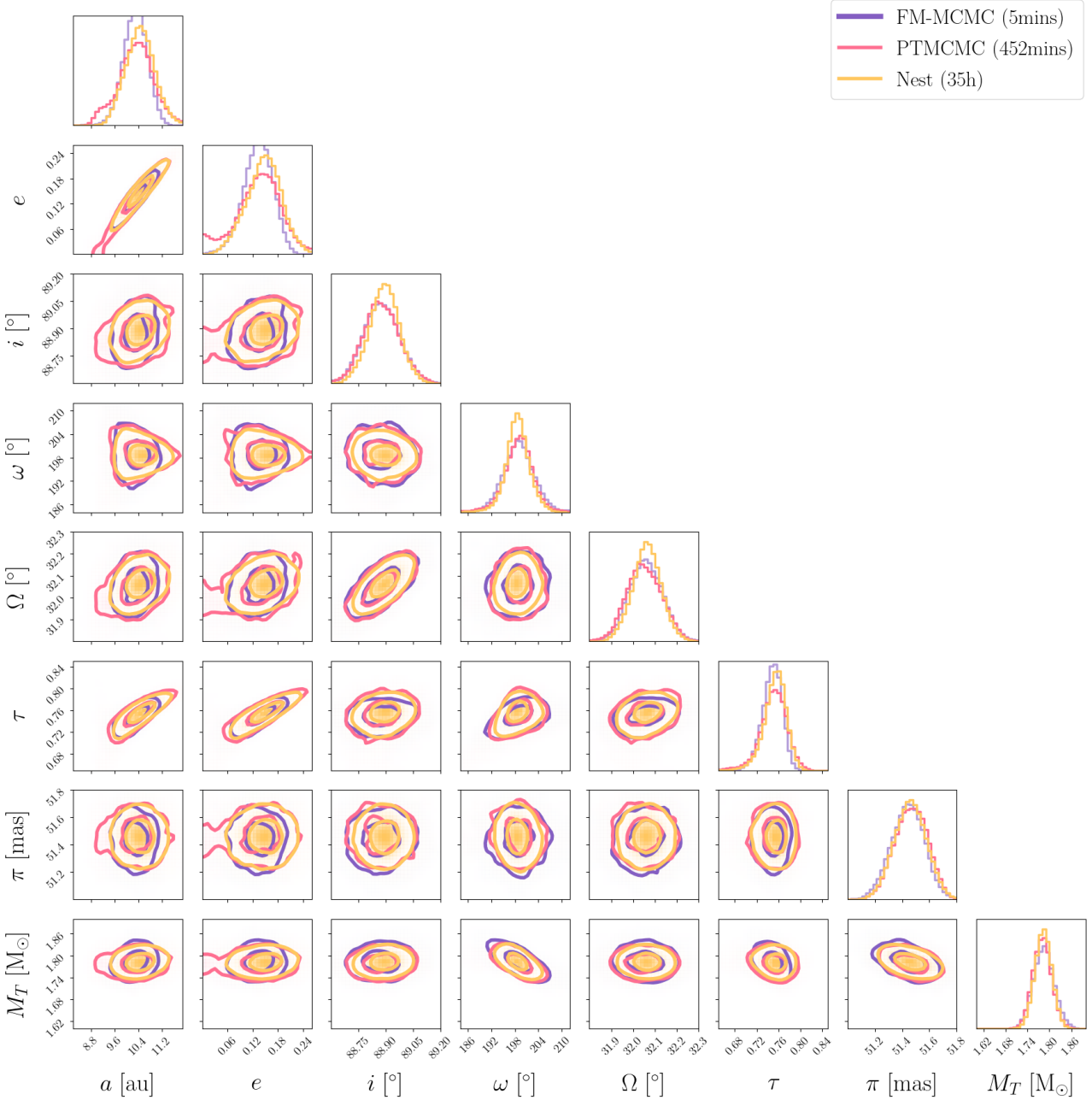


Fig. 4 FM-MCMC vs PTMCMC vs Nested sampling posterior comparison for β -Pictoris b orbital elements. Posterior distributions of β -Pictoris b's orbital parameters inferred by FM-MCMC (blue), PTMCMC (orange), and nested sampling (red) show statistical consistency, with nearly identical $1 - \sigma$ and $2 - \sigma$ credible regions. This overlap demonstrates that FM-MCMC accurately reproduces the full posterior structure obtained by conventional sampling methods.

in Table 3, are consistent with results obtained from PTMCMC and Nested Sampling, confirming the fidelity of the inferred distributions. Moreover, likelihood comparisons (Table 2) show that FM-MCMC achieves a mean negative log-likelihood of -133.0 , which is **53.4% better** than that of PTMCMC (-285.4) and **43.2% better** than that of Nested sampling (-234.3), underscoring its superior capability to explore complex, high-dimensional parameter spaces. Critically, its **maximum likelihood** (-129.6) equals PTMCMC (-129.6) and deviates only **0.08%** from Nested sampling (-129.5), demonstrating that FM-MCMC achieves enhanced efficiency without optimality.

FM-MCMC achieves high efficiency by integrating machine learning with traditional sampling. Under identical configurations (20 temperature tiers, 1,000 parallel chains), FM-MCMC completes sampling in **348.9 seconds** (≈ 5.8 minutes), outperforming PTMCMC (27,133.9s/7.5h) and Nested sampling (127,478.8s/35.4h) by **77.8x** and **365.4x**, respectively (Table 2).

The sub-6-minute inference speed of FM-MCMC (Table 2) transforms the study of dynamically active systems by enabling daily orbital updates during intensive observation campaigns. This rapid posterior estimation of β Pictoris b's orbital parameters is particularly valuable: it allows timely scheduling of follow-up spectroscopic observations with JWST to probe the planet's atmospheric CH_4/CO ratio [67], provides precise constraints on dynamical interactions with

the debris disk through real-time N-body simulations [68, 69], and offers informed priors to facilitate the search for additional companions, such as the hypothesized β -Pictoris c [70].

Table 3 Posterior estimates of β Pictoris b’s Keplerian parameters using PTMCMC, Nested sampling, and FM-MCMC methods. All values show median with 1σ confidence intervals.

Parameter	PTMCMC	Nested sampling	FM-MCMC
a	$10.34^{+0.56}_{-0.57}$	$10.46^{+0.56}_{-0.57}$	$10.31^{+0.37}_{-0.39}$
e	$0.14^{+0.05}_{-0.05}$	$0.15^{+0.04}_{-0.04}$	$0.13^{+0.03}_{-0.04}$
i	$88.87^{+0.10}_{-0.09}$	$88.89^{+0.08}_{-0.08}$	$88.87^{+0.10}_{-0.09}$
ω	$198.91^{+3.23}_{-3.92}$	$198.60^{+2.72}_{-2.54}$	$198.87^{+3.97}_{-3.72}$
Ω	$32.05^{+0.08}_{-0.08}$	$32.06^{+0.06}_{-0.06}$	$32.06^{+0.08}_{-0.08}$
τ	$0.75^{+0.02}_{-0.03}$	$0.75^{+0.02}_{-0.02}$	$0.75^{+0.02}_{-0.02}$
π	$51.47^{+0.11}_{-0.12}$	$51.46^{+0.11}_{-0.12}$	$51.44^{+0.11}_{-0.12}$
M_T	$1.78^{+0.02}_{-0.02}$	$1.78^{+0.02}_{-0.02}$	$1.78^{+0.03}_{-0.03}$

5 Conclusion and Discussion

We have presented FM-MCMC, a flow-matching enhanced MCMC sampler for astrometric orbit fitting, and demonstrated its application to the well-studied β Pictoris b system. FM-MCMC produces posterior distributions that are statistically consistent with those obtained via fully converged PTMCMC and nested sampling, while achieving a roughly $100\times$ reduction in wall-clock runtime. Importantly, this substantial speed-up is achieved without sacrificing the accuracy of the posterior estimates. By integrating learned transport maps into a conventional MCMC sampler, FM-MCMC unites the statistical rigor of Bayesian inference with the high computational efficiency characteristic of modern generative models.

While our study focused on β Pictoris b using priors consistent with previous works, FM-MCMC shows promise for application to broader prior ranges, multi-planet systems, and entirely new scientific problems. Trained once on simulated astrometric datasets covering extensive parameter spaces, the flow-matching component enables rapid posterior estimation with limited prior knowledge, thus paving the way for systematic orbit characterization of directly imaged companions without further sampler adjustments.

In the future, the FM-MCMC paradigm can be adapted to other exoplanet detection modalities beyond direct imaging. By constructing multi-modal embeddings of heterogeneous datasets—such as transits, radial velocities, and astrometry—one can train unified flows that act as efficient proposal distributions for joint parameter estimation. This multi-modal inference framework has the potential to streamline analysis pipelines for upcoming missions, ultimately enabling rapid and uncertainty-aware characterization of exoplanet orbital dynamics.

Acknowledgements. This study is supported by the National Key Research and Development Program of China (Grant No. 2021YFC2201901, Grant No. 2021YFC2203004, Grant No. 2020YFC2200100 and Grant No. 2021YFC2201903). International Partnership Program of the Chinese Academy of Sciences, Grant No. 025GJHZ2023106GC. We also gratefully acknowledge the financial support from Brazilian agencies Fundação de Amparo à Pesquisa do Estado de São Paulo (FAPESP), Fundação de Amparo à Pesquisa do Estado do Rio Grande do Sul (FAPERGS), Fundação de Amparo à Pesquisa do Estado do Rio de Janeiro (FAPERJ), Conselho Nacional de Desenvolvimento Científico e Tecnológico (CNPq), and Coordenação de Aperfeiçoamento de Pessoal de Nível Superior (CAPES). This work is also supported by High-performance Computing Platform of Peking University.

Data Availability. The data generated and analyzed during this study are available from the corresponding author upon reasonable request.

Code Availability. The code used in this study is available from the corresponding author upon reasonable request.

Competing Interests. The authors declare no competing interests.

References

[1] Wolszczan, A., Frail, D.A.: A planetary system around the millisecond pulsar PSR1257 + 12. *Nature* **355**(6356), 145–147 (1992) <https://doi.org/10.1038/355145a0>

[2] Mayor, M., Queloz, D.: A Jupiter-mass companion to a solar-type star. *Nature* **378**(6555), 355–359 (1995) <https://doi.org/10.1038/378355a0>

[3] NASA Exoplanet Archive: NASA Exoplanet Archive by the data 2025.07.09. <https://science.nasa.gov/exoplanets/>. Accessed: 2025-09-05 (2025)

[4] Howe, A.R., Becker, J.C., Stark, C.C., Adams, F.C.: Architecture classification for extrasolar planetary systems. arXiv preprint arXiv:2501.08191 (2025)

[5] Brandt, T.D., Dupuy, T.J., Li, Y., Brandt, G.M., Zeng, Y., Michalik, D., Bardalez Gagliuffi, D.C., Raposo-Pulido, V.: orvara: An efficient code to fit orbits using radial velocity, absolute, and/or relative astrometry. *The Astronomical Journal* **162**(5), 186 (2021) <https://doi.org/10.3847/1538-3881/ac042e>

[6] Blunt, S., Wang, J.J., Angelo, I., Ngo, H., Cody, D., De Rosa, R.J., Graham, J.R., Hirsch, L., Nagpal, V., Nielsen, E.L., Pearce, L., Rice, M., Tejada, R.: orbitize!: A comprehensive orbit-fitting software package for the high-contrast imaging community. *The Astronomical Journal* **159**(3), 89 (2020) <https://doi.org/10.3847/1538-3881/ab6663>

[7] Winn, J.N.: The Transiting Exoplanet Survey Satellite (2024). <https://arxiv.org/abs/2410.12905>

[8] Fortier, A., Simon, A.E., Broeg, C., Olofsson, G., Deline, A., Wilson, T.G., Maxted, P.F.L., Brandeker, A., Cameron, A.C., Beck, M., Bekkelien, A., Billot, N., Bonfanti, A., Bruno, G., Cabrera, J., Delrez, L., Demory, B.-O., Futyani, D., Florén, H.-G., Günther, M.N., Heitzmann, A., Hoyer, S., Isaak, K.G., Sousa, S.G., Stalport, M., Turin, A., Verhoeve, P., Akinsanmi, B., Alibert, Y., Alonso, R., Bánhidi, D., Bárczy, T., Barrado, D., Barros, S.C., Baumjohann, W., Baycroft, T., Beck, T., Benz, W., Bíró, B.I., Bódi, A., Bonfils, X., Borsato, L., Charnoz, S., Cseh, B., Csizmadia, S., Csányi, I., Cubillos, P.E., Davies, M.B., Davis, Y.T., Deleuil, M., Demangeon, O.D.S., Derekas, A., Dransfield, G., Ducrot, E., Ehrenreich, D., Erikson, A., Fariña, C., Fossati, L., Fridlund, M., Gandolfi, D., Garai, Z., Garcia, L., Gillon, M., Chew, Y.G.M., Gómez-Muñoz, M.A., Granata, V., Güdel, M., Guterman, P., Hegedüs, T., Helling, C., Jehin, E., Kalup, C., Kilkenny, D., Kiss, L., Kriskovics, L., Lam, K.W.F., Laskar, J., Etangs, A.L., Lendl, M., Pina, A.L., Luntzer, A., Magrin, D., Miller, N.J., Contreras, D.M., Mordasini, C., Munari, M., Murray, C.A., Nascimbeni, V., Ottacher, H., Ottensamer, R., Pagano, I., Pál, A., Pallé, E., Pasetti, A., Pedersen, P., Peter, G., Petrucci, R., Piotto, G., Pizarro-Rubio, A., Pollacco, D., Pribulla, T., Queloz, D., Ragazzoni, R., Rando, N., Rauer, H., Ribas, I., Sabin, L., Santos, N.C., Scandariato, G., Schanche, N., Schröfenegger, U., Scutt, O.J., Sebastian, D., Ségransan, D., Seli, B., Smith, A.M.S., Southworth, R., Standing, M.R., Szabó, M.G., Szakáts, R., Thomas, N., Timmermans, M., Triaud, A.H.M.J., Udry, S., Grootel, V.V., Venturini, J., Villaver, E., Vinkó, J., Walton, N.A., Wells, R., Wolter, D.: CHEOPS in-flight performance: A comprehensive look at the first 3.5 years of operations (2024). <https://arxiv.org/abs/2406.01716>

[9] Pancino, E.: Gaia: The galaxy in six (and more) dimensions. *Advances in Space Research* **65**(1), 1–10 (2020) <https://doi.org/10.1016/j.asr.2019.11.007>

[10] Beuzit, J.-L., Vigan, A., Mouillet, D., Dohlen, K., Gratton, R., Boccaletti, A., Sauvage, J.-F., Schmid, H.M., Langlois, M., Petit, C., *et al.*: Sphere: the exoplanet imager for the very large telescope. *Astronomy & Astrophysics* **631**, 155 (2019)

[11] Rauer, H., Aerts, C., Cabrera, J., Deleuil, M., Erikson, A., Gizon, L., Goupil, M., Heras, A., Lorenzo-Alvarez, J., Marliani, F., Martin-Garcia, C., Mas-Hesse, J.M., O'Rourke, L., Osborn, H., Pagano, I., Piotto, G.: The PLATO Mission (2024). <https://arxiv.org/abs/2406.05447>

[12] Changeat, Q., Yip, K.H.: ESA-Ariel Data Challenge NeurIPS 2022: Introduction to exo-atmospheric studies and presentation of the Atmospheric Big Challenge (ABC) Database (2023). <https://arxiv.org/abs/2206.14633>

[13] Zingales, T., Tinetti, G., Pillitteri, I., Leconte, J., Micela, G., Sarkar, S.: The ariel mission reference sample. *Experimental Astronomy* **46**, 67–100 (2017)

[14] Boccaletti, A., Chauvin, G., Mouillet, D., Absil, O., Allard, F., Antoniucci, S., Augereau, J.-C., Barge, P., Barufolo, A., Baudino, J.-L., Baudoz, P., Beaulieu, M., Benisty, M., Beuzit, J.-L., Bianco, A., Biller, B., Bonavita, B., Bonnefoy, M., Bos, S., Bouret, J.-C., Brandner, W., Buchschache, N., Carry, B., Cantalloube, F., Cascone, E., Carlotti, A., Charnay, B., Chiavassa, A., Choquet, E., Clenet, Y., Crida, A., De Boer, J., De Caprio, V., Desidera, S., Desert, J.-M., Delisle, J.-B., Delorme, P., Dohlen, K., Doelman, D., Dominik, C., Orazi, V.D., Dougados, C., Doute, S., Fedele, D., Feldt, M., Ferreira, F., Fontanive, C., Fusco, T., Galicher, R., Garufi, A., Gendron, E., Ghedina, A., Ginski, C., Gonzalez, J.-F., Gratadour, D., Gratton, R., Guillot, T., Haffert, S., Hagelberg, J., Henning, T.,

Huby, E., Janson, M., Kamp, I., Keller, C., Kenworthy, M., Kervella, P., Kral, Q., Kuhn, J., Lagadec, E., Laibe, G., Langlois, M., Lagrange, A.-M., Launhardt, R., Leboulleux, L., Le Coroller, H., Li Causi, G., Loupias, M., Maire, A.L., Marleau, G., Martinache, F., Martinez, P., Mary, D., Mattioli, M., Mazoyer, J., Meheut, H., Menard, F., Mesa, D., Meunier, N., Miguel, Y., Milli, J., Min, M., Molliere, P., Mordasini, C., Moretto, G., Mugnier, L., Muro Arena, G., Nardetto, N., Diaye, M.N., Nesvadba, N., Pedichini, F., Pinilla, P., Por, E., Potier, A., Quanz, S., Rameau, J., Roelfsema, R., Rouan, D., Rigliaco, E., Salasnich, B., Samland, M., Sauvage, J.-F., Schmid, H.-M., Segransan, D., Snellen, I., Snik, F., Soulez, F., Stadler, E., Stam, D., Tallon, M., Thebault, P., Thiebaut, E., Tschudi, C., Udry, S., van Holstein, R., Vernazza, P., Vidal, F., Vigan, A., Waters, R., Wildi, F., Willson, M., Zanutta, A., Zavagno, A., Zurlo, A.: SPHERE+: Imaging young Jupiters down to the snowline. arXiv e-prints, 2003–05714 (2020) <https://doi.org/10.48550/arXiv.2003.05714> arXiv:2003.05714 [astro-ph.EP]

[15] Bailey, V.P., Bendek, E., Monacelli, B., Baker, C., Bedrosian, G., Cady, E., Douglas, E.S., Groff, T., Hildebrandt, S.R., Kasdin, N.J., Krist, J., Macintosh, B., Mennesson, B., Morrissey, P., Poberezhskiy, I., Subedi, H.B., Rhodes, J., Roberge, A., Ygouf, M., Zellem, R.T., Zhao, F., Zimmerman, N.T.: Nancy Grace Roman Space Telescope Coronagraph Instrument Overview and Status (2023). <https://arxiv.org/abs/2309.08672>

[16] Maire, A.-L., Delrez, L., Pozuelos, F.J., Becker, J., Espinoza, N., Lillo-Box, J., Revol, A., Absil, O., Agol, E., Almenara, J.M., *et al.*: Workshop summary: Exoplanet orbits and dynamics. Publications of the Astronomical Society of the Pacific **135**(1052), 106001 (2023)

[17] Fischer, D.A., Howard, A.W., Laughlin, G.P., Macintosh, B., Mahadevan, S., Sahlmann, J., Yee, J.C.: Exoplanet Detection Techniques. In: Beuther, H., Klessen, R.S., Dullemond, C.P., Henning, T. (eds.) Protostars and Planets VI, pp. 715–737 (2014). https://doi.org/10.2458/azu_uapress_9780816531240-ch031

[18] Deeg, H.J., Belmonte, J.A.: Handbook of Exoplanets, (2018). <https://doi.org/10.1007/978-3-319-55333-7>

[19] Abuter, R., Accardo, M., Amorim, A., Anugu, N., Avila, G., Azouaoui, N., Benisty, M., Berger, J.-P., Blind, N., Bonnet, H., *et al.*: First light for gravity: Phase referencing optical interferometry for the very large telescope interferometer. *Astronomy & Astrophysics* **602**, 94 (2017)

[20] Lightsey, P.A., Atkinson, C., Clampin, M., Feinberg, L.D.: James webb space telescope: large deployable cryogenic telescope in space. *Optical Engineering* **51**(1), 011003–011003 (2012)

[21] Forveille, T., Beuzit, J.L., Delfosse, X., Segransan, D., Beck, F., Mayor, M., Perrier, C., Tokovini, A., Udry, S.: Accurate masses of very low mass stars: I Gl 570BC (0.6+0.4 Msol) (1999). <https://arxiv.org/abs/astro-ph/9909342>

[22] Blunt, S., Nielsen, E.L., De Rosa, R.J., Konopacky, Q.M., Ryan, D., Wang, J.J., Pueyo, L., Rameau, J., Marois, C., Marchis, F., Macintosh, B., Graham, J.R., Duchêne, G., Schneider, A.C.: Orbits for the Impatient: A Bayesian Rejection-sampling Method for Quickly Fitting the Orbits of Long-period Exoplanets. *AJ* **153**(5), 229 (2017) <https://doi.org/10.3847/1538-3881/aa6930> arXiv:1703.10653 [astro-ph.EP]

[23] Foreman-Mackey, D., Hogg, D.W., Lang, D., Goodman, J.: emcee: The MCMC Hammer. *PASP* **125**(925), 306 (2013) <https://doi.org/10.1086/670067> arXiv:1202.3665 [astro-ph.IM]

[24] Vousden, W.D., Farr, W.M., Mandel, I.: Dynamic temperature selection for parallel tempering in Markov chain Monte Carlo simulations. *MNRAS* **455**(2), 1919–1937 (2016) <https://doi.org/10.1093/mnras/stv2422> arXiv:1501.05823 [astro-ph.IM]

[25] Speagle, J.S.: dynesty: a dynamic nested sampling package for estimating bayesian posteriors and evidences. *Monthly Notices of the Royal Astronomical Society* **493**(3), 3132–3158 (2020) <https://doi.org/10.1093/mnras/staa278> <https://academic.oup.com/mnras/article-pdf/493/3/3132/32890730/staa278.pdf>

[26] Sun, H., Bouman, K.L., Tiede, P., Wang, J.J., Blunt, S., Mawet, D.: Alpha-deep probabilistic inference (alpha-dpi): Efficient uncertainty quantification from exoplanet astrometry to black hole feature extraction. *The Astrophysical Journal* **932**(2), 99 (2022) <https://doi.org/10.3847/1538-4357/ac6be9>

[27] Ruth, M.: Exoplanet Orbital Characterization Using Simulation-Based Inference. PhD thesis, University of Liège, Liège, Belgium (June 2024). <https://matheo.uliege.be/handle/2268.2/20393>

[28] Chen, C., Kong, L., Li, G., Tao, M.: Deeptv: Deep learning prediction of hidden exoplanet from transit timing variations. arXiv preprint arXiv:2409.04557 (2024)

[29] Sithajan, S., Meethong, S.: Applied machine-learning models to identify spectral sub-types of m dwarfs from

[30] Ofman, L., Averbuch, A., Shliselberg, A., Benaun, I., Segev, D., Rissman, A.: Automated identification of transiting exoplanet candidates in nasa transiting exoplanets survey satellite (tess) data with machine learning methods. ArXiv [abs/2102.10326](https://arxiv.org/abs/2102.10326) (2021)

[31] Du, M., Liang, B., Wang, H., Xu, P., Luo, Z., Wu, Y.: Advancing space-based gravitational wave astronomy: Rapid parameter estimation via normalizing flows. Science China Physics, Mechanics & Astronomy **67**(3), 230412 (2024)

[32] Liang, B., Du, M., Wang, H., Xu, Y., Liu, C., Wei, X., Xu, P., Qiang, L.-e., Luo, Z.: Rapid parameter estimation for merging massive black hole binaries using continuous normalizing flows. Machine Learning: Science and Technology **5**(4), 045040 (2024) <https://doi.org/10.1088/2632-2153/ad8da9>

[33] Liang, B., Liu, C., Zhao, T., Du, M., Liang, M., Shi, R., Guo, H., Xu, Y., Qiang, L.-e., Xu, P., Qian, W.-L., Luo, Z.: Accelerating Stochastic Gravitational Wave Backgrounds Parameter Estimation in Pulsar Timing Arrays with Flow Matching (2024). <https://arxiv.org/abs/2412.19169>

[34] Wang, K., Ge, J., Willis, K., Wang, K., Zhao, Y.: The gpu phase folding and deep learning method for detecting exoplanet transits. Monthly Notices of the Royal Astronomical Society **528**(3), 4053–4067 (2024) <https://doi.org/10.1093/mnras/stae245> <https://academic.oup.com/mnras/article-pdf/528/3/4053/56617446/stae245.pdf>

[35] Pan, J.-S., Ting, Y.-S., Yu, J.: Astroconformer: The prospects of analysing stellar light curves with transformer-based deep learning models. Monthly Notices of the Royal Astronomical Society **528**(4), 5890–5903 (2024) <https://doi.org/10.1093/mnras/stae068> <https://academic.oup.com/mnras/article-pdf/528/4/5890/56707271/stae068.pdf>

[36] Prithivraj, G., Kumari, A.: Identification and classification of exoplanets using machine learning techniques. ArXiv [abs/2305.09596](https://arxiv.org/abs/2305.09596) (2023)

[37] Ulaş, B., Szklenár, T., Szabó, R.: Detection of Oscillation-like Patterns in Eclipsing Binary Light Curves using Neural Network-based Object Detection Algorithms (2025). <https://arxiv.org/abs/2501.17538>

[38] Poleo, V.T., Eisner, N., Hogg, D.W.: NotPlaNET: Removing False Positives from Planet Hunters TESS with Machine Learning (2024). <https://arxiv.org/abs/2405.18278>

[39] Wald, C., Steidl, G.: Flow Matching: Markov Kernels, Stochastic Processes and Transport Plans (2025). <https://arxiv.org/abs/2501.16839>

[40] Durkan, C., Bekasov, A., Murray, I., Papamakarios, G.: Neural spline flows. Advances in neural information processing systems **32** (2019)

[41] Dinh, L., Sohl-Dickstein, J., Bengio, S.: Density estimation using real NVP. In: International Conference on Learning Representations (2017). <https://openreview.net/forum?id=HkpbnH9lx>

[42] Dinh, L., Krueger, D., Bengio, Y.: Nice: Non-linear independent components estimation. arXiv: Learning (2014)

[43] Chen, T.Q., Rubanova, Y., Bettencourt, J., Duvenaud, D.K.: Neural ordinary differential equations. In: Neural Information Processing Systems (2018). <https://api.semanticscholar.org/CorpusID:49310446>

[44] Chen, R.T.Q., Amos, B., Nickel, M.: Learning neural event functions for ordinary differential equations. International Conference on Learning Representations (2021)

[45] Kidger, P., Chen, R.T.Q., Lyons, T.J.: "hey, that's not an ode": Faster ode adjoints via seminorms. International Conference on Machine Learning (2021)

[46] Chen, R.T.Q.: torchdiffeq (2018). <https://github.com/rtqichen/torchdiffeq>

[47] Dax, M., Wildberger, J., Buchholz, S., Green, S.R., Macke, J.H., Schölkopf, B.: Flow Matching for Scalable Simulation-Based Inference (2023). <https://arxiv.org/abs/2305.17161>

[48] Tejero-Cantero, A., Boelts, J., Deistler, M., Lueckmann, J.-M., Durkan, C., Gonçalves, P.J., Greenberg, D.S., Macke, J.H.: sbi: A toolkit for simulation-based inference. Journal of Open Source Software **5**(52), 2505 (2020) <https://doi.org/10.21105/joss.02505>

[49] Viscasillas Vázquez, C., Solano, E., Ulla, A., Ambrosch, M., Álvarez, M. A., Manteiga, M., Magrini, L., Santoveña-Gómez, R., Dafonte, C., Pérez-Fernández, E., Aller, A., Drazdauskas, A., Mikolaitis, Š., Rodrigo, C.: Advanced classification of hot subdwarf binaries using artificial intelligence techniques and gaia dr3 data. *A & A* **691**, 223 (2024) <https://doi.org/10.1051/0004-6361/202451247>

[50] Vida, Krisztián, Bódi, Attila, Szklenár, Tamás, Seli, Bálint: Finding flares in kepler and tess data with recurrent deep neural networks. *A & A* **652**, 107 (2021) <https://doi.org/10.1051/0004-6361/202141068>

[51] Smith, J.: Astrometric binary classification via artificial neural networks. *ArXiv* **abs/2409.09563** (2024)

[52] Sahlmann, J., Gómez, P.: Machine learning-based identification of gaia astrometric exoplanet orbits. *Monthly Notices of the Royal Astronomical Society* **537**(2), 1130–1145 (2025) <https://doi.org/10.1093/mnras/staf018> <https://academic.oup.com/mnras/article-pdf/537/2/1130/61382466/staf018.pdf>

[53] Liu, X., Gong, C., liu: Flow straight and fast: Learning to generate and transfer data with rectified flow. In: *The Eleventh International Conference on Learning Representations* (2023). <https://openreview.net/forum?id=XVjTT1nw5z>

[54] Lipman, Y., Chen, R.T.Q., Ben-Hamu, H., Nickel, M., Le, M.: Flow matching for generative modeling. In: *The Eleventh International Conference on Learning Representations* (2023). <https://openreview.net/forum?id=PqvMRDCJ9t>

[55] Papamakarios, G., Murray, I.: Fast ε -free inference of simulation models with bayesian conditional density estimation. *Advances in neural information processing systems* **29** (2016)

[56] Lueckmann, J.-M., Goncalves, P.J., Bassetto, G., Öcal, K., Nonnenmacher, M., Macke, J.H.: Flexible statistical inference for mechanistic models of neural dynamics (2017). <https://arxiv.org/abs/1711.01861>

[57] Gabrié, M., Rotskoff, G.M., Vanden-Eijnden, E.: Adaptive monte carlo augmented with normalizing flows. *Proceedings of the National Academy of Sciences* **119**(10), 2109420119 (2022) <https://doi.org/10.1073/pnas.2109420119> <https://www.pnas.org/doi/pdf/10.1073/pnas.2109420119>

[58] Wong, K.W.K., Gabrié, M., Foreman-Mackey, D.: flowMC: Normalizing flow enhanced sampling package for probabilistic inference in JAX. *J. Open Source Softw.* **8**(83), 5021 (2023) <https://doi.org/10.21105/joss.05021> [arXiv:2211.06397](https://arxiv.org/abs/2211.06397) [astro-ph.IM]

[59] Gabrié, M., Rotskoff, G.M., Vanden-Eijnden, E.: Adaptive Monte Carlo augmented with normalizing flows. *Proc. Nat. Acad. Sci.* **119**(10), 2109420119 (2022) <https://doi.org/10.1073/pnas.2109420119> [arXiv:2105.12603](https://arxiv.org/abs/2105.12603) [physics.data-an]

[60] Lagrange, A.-M., *et al.*: A probable giant planet imaged in the Beta Pictoris disk. *Astron. Astrophys.* **493**, 21 (2009) <https://doi.org/10.1051/0004-6361:200811325> [arXiv:0811.3583](https://arxiv.org/abs/0811.3583) [astro-ph]

[61] Lagrange, A.-M., *et al.*: A giant planet imaged in the disk of the young star Beta Pictoris. *Science* **329**, 57 (2010) <https://doi.org/10.1126/science.1187187> [arXiv:1006.3314](https://arxiv.org/abs/1006.3314) [astro-ph.EP]

[62] Nielsen, E.L., Liu, M.C., Wahhaj, Z., Biller, B.A., Hayward, T.L., Males, J.R., Close, L.M., Morzinski, K.M., Skemer, A.J., Kuchner, M.J., Rodigas, T.J., Hinz, P.M., Chun, M., Ftaclas, C., Toomey, D.W.: The Gemini NICI Planet-Finding Campaign: The Orbit of the Young Exoplanet β Pictoris b. *ApJ* **794**(2), 158 (2014) <https://doi.org/10.1088/0004-637X/794/2/158> [arXiv:1403.7195](https://arxiv.org/abs/1403.7195) [astro-ph.EP]

[63] Lagrange, A.-M., Boccaletti, A., Langlois, M., Chauvin, G., Gratton, R., Beust, H., Desidera, S., Milli, J., Bonnefoy, M., Cheetham, A., Feldt, M., Meyer, M., Vigan, A., Biller, B., Bonavita, M., Baudino, J.-L., Cantalloube, F., Cudel, M., Daemgen, S., Delorme, P., D’Orazi, V., Girard, J., Fontanive, C., Hagelberg, J., Janson, M., Kepler, M., Kopytova, T., Galicher, R., Lannier, J., Le Coroller, H., Ligi, R., Maire, A.-L., Mesa, D., Messina, S., Müller, A., Peretti, S., Perrot, C., Rouan, D., Salter, G., Samland, M., Schmidt, T., Sissa, E., Zurlo, A., Beuzit, J.-L., Mouillet, D., Dominik, C., Henning, T., Lagadec, E., Ménard, F., Schmid, H.-M., Turatto, M., Udry, S., Bohn, A.J., Charnay, B., Gomez Gonzales, C.A., Gry, C., Kenworthy, M., Kral, Q., Mordasini, C., Moutou, C., van der Plas, G., Schlieder, J.E., Abe, L., Antichi, J., Baruffolo, A., Baudoz, P., Baudrand, J., Blanchard, P., Bazzon, A., Buey, T., Carillet, M., Carle, M., Charton, J., Cascone, E., Claudi, R., Costille, A., Deboulbe, A., De Caprio, V., Dohlen, K., Fantinel, D., Feautrier, P., Fusco, T., Gigan, P., Giro, E., Gisler, D., Gluck, L., Hubin, N., Hugot, E., Jaquet, M., Kasper, M., Madec, F., Magnard, Y., Martinez, P., Maurel, D., Le Mignant, D., Möller-Nilsson, O., Llored, M., Moulin, T., Origné, A., Pavlov, A., Perret, D., Petit, C., Pragt, J., Szulagyi, J., Wildi, F.: Post-conjunction

detection of β Pictoris b with VLT/SPHERE. *A&A* **621**, 8 (2019) <https://doi.org/10.1051/0004-6361/201834302> arXiv:1809.08354 [astro-ph.EP]

[64] Nielsen, E.L., De Rosa, R.J., Wang, J.J., Sahlmann, J., Kalas, P., Duchêne, G., Rameau, J., Marley, M.S., Saumon, D., Macintosh, B., Millar-Blanchaer, M.A., Nguyen, M.M., Ammons, S.M., Bailey, V.P., Barman, T., Bulger, J., Chilcote, J., Cotten, T., Doyon, R., Esposito, T.M., Fitzgerald, M.P., Follette, K.B., Gerard, B.L., Goodsell, S.J., Graham, J.R., Greenbaum, A.Z., Hibon, P., Hung, L.-W., Ingraham, P., Konopacky, Q., Larkin, J.E., Maire, J., Marchis, F., Marois, C., Metchev, S., Oppenheimer, R., Palmer, D., Patience, J., Perrin, M., Poyneer, L., Pueyo, L., Rajan, A., Rantakyrö, F.T., Ruffio, J.-B., Savransky, D., Schneider, A.C., Sivaramakrishnan, A., Song, I., Soummer, R., Thomas, S., Wallace, J.K., Ward-Duong, K., Wiktorowicz, S., Wolff, S.: The Gemini Planet Imager Exoplanet Survey: Dynamical Mass of the Exoplanet β Pictoris b from Combined Direct Imaging and Astrometry. *AJ* **159**(2), 71 (2020) <https://doi.org/10.3847/1538-3881/ab5b92> arXiv:1911.11273 [astro-ph.EP]

[65] Lagrange, A.-M., Meunier, N., Rubini, P., Keppler, M., Galland, F., Chapellier, E., Michel, E., Balona, L., Beust, H., Guillot, T., Grandjean, A., Borgniet, S., Mékarnia, D., Wilson, P.A., Kiefer, F., Bonnefoy, M., Lillo-Box, J., Pantoja, B., Jones, M., Iglesias, D.P., Rodet, L., Diaz, M., Zapata, A., Abe, L., Schmider, F.-X.: Evidence for an additional planet in the β Pictoris system. *Nature Astronomy* **3**, 1135–1142 (2019) <https://doi.org/10.1038/s41550-019-0857-1>

[66] Green, R.M.: *Spherical Astronomy*. Cambridge University Press, ??? (1985)

[67] Hayoz, J., Cugno, G., Quanz, S.P., Patapis, P., Alei, E., Bonse, M.J., Dannert, F.A., Garvin, E.O., Gebhard, T.D., Konrad, B.S., Sartori, L.F.: Crocodile: Incorporating medium-resolution spectroscopy of close-in directly imaged exoplanets into atmospheric retrievals via cross-correlation. *Astronomy & Astrophysics* **678** (2023) <https://doi.org/10.1051/0004-6361/202245752>

[68] Belleman, R.G., Bédorf, J., Portegies Zwart, S.F.: High performance direct gravitational n-body simulations on graphics processing units ii: An implementation in cuda. *New Astronomy* **13**(2), 103–112 (2008) <https://doi.org/10.1016/j.newast.2007.07.004>

[69] Lacquement, A., Beust, H., Faramaz-Gorka, V., Duchêne, G.: Dynamics of the beta pictoris planetary system and possibility of an additional planet. *Astronomy & Astrophysics* **694**, 236 (2025) <https://doi.org/10.1051/0004-6361/202452632>

[70] Lacour, S., Wang, J.J., Rodet, L., Nowak, M., Shangguan, J., Beust, H., Lagrange, A.-M., Abuter, R., Amorim, A., Asensio-Torres, R., Benisty, M., Berger, J.-P., Blunt, S., Boccaletti, A., Bohn, A., Bolzer, M.-L., Bonnefoy, M., Bonnet, H., Bourdarot, G., Brandner, W., Cantalloube, F., Caselli, P., Charnay, B., Chauvin, G., Choquet, E., Christiaens, V., Clénet, Y., Foresto, V., Cridland, A., Dembet, R., Dexter, J., Zeeuw, P.T., Drescher, A., Duvert, G., Eckart, A., Eisenhauer, F., Gao, F., Garcia, P., Garcia Lopez, R., Gendron, E., Genzel, R., Gillessen, S., Girard, J.H., Haubois, X., Heißen, G., Henning, T., Hinkley, S., Hippler, S., Horrobin, M., Houllé, M., Hubert, Z., Jocou, L., Kammerer, J., Keppler, M., Kervella, P., Kreidberg, L., Lapeyrère, V., Le Bouquin, J.-B., Léna, P., Lutz, D., Maire, A.-L., Mérard, A., Mollière, P., Monnier, J.D., Mouillet, D., Nasedkin, E., Ott, T., Otten, G.P.P.L., Paladini, C., Paumard, T., Perraut, K., Perrin, G., Pfuhl, O., Rickman, E., Pueyo, L., Rameau, J., Rousset, G., Rustamkulov, Z., Samland, M., Shimizu, T., Sing, D., Stadler, J., Stolker, T., Straub, O., Straubmeier, C., Sturm, E., Tacconi, L.J., Dishoeck, E.F., Vigan, A., Vincent, F., Fellenberg, S.D., Ward-Duong, K., Widmann, F., Wiprecht, E., Wiezorek, E., Woillez, J., Yazici, S., Young, A.: The mass of betapictoris c from betapictoris b orbital motion. *Astronomy & Astrophysics* **654**, 2 (2021) <https://doi.org/10.1051/0004-6361/202141889>